XLVI CILAMCE
VITÓRIA - ES - BRAZIL - 2025
XLVI IBERO-LATIN AMERICAN CONGRESS ON COMPUTATIONAL METHODS IN ENGINEERING

Numerical Modeling for the Characterization of Fractured Damage Zones in Geological Faults

Amanda Scherer de Brito[1,2], Roberto Quevedo[2], Deane Roehl[1,2], Bruno R.B.M. Carvalho[3]

[1] *Civil and Environmental Engineering Department, PUC-Rio*
Rua Marquês de São Vicente, 225, 22453-900, Rio de Janeiro, Brazil
amandascherer@aluno.puc-rio.br, droehl@puc-rio.br
[2] *Tecgraf Institute, PUC-Rio*
Rua Marquês de São Vicente, 225, 22453-900, Rio de Janeiro, Brazil
amandascherer @tecgraf.puc-rio.br, rquevedo@tecgraf.puc-rio.br, deane@tecgraf.puc-rio.br
[3]*Petrobras Research Center*
Av. Horácio Macedo, 950, 21941-915, Rio de Janeiro, Brazil
brcarvalho@petrobras.com.br

Abstract. In the oil and gas industry, geological faults play an essential role in compartmentalizing reservoirs. However, faults are made up of impermeable surfaces and adjacent damage zones made up of fracture networks that can result in preferential paths for fluid migration. Therefore, properly characterizing these zones is important for defining more efficient production strategies in oil fields. In this sense, some approaches based on numerical modeling that consider the damage zone as a continuous domain using the finite element method and elastoplastic constitutive models have been proposed. Other approaches are based on the fracture mechanics theory, considering elastic models to evaluate fracture occurrence, orientation, and propagation. However, fracture networks usually present in damage zones in geological faults are not explicitly modeled, leaving uncertainty related to the characterization of these fractures for subsequent flow modeling. Given this scenario, this study proposes developing numerical models applied to geological faults, focusing on the explicit representation of fractures by including cohesive interface elements in the modeling with the finite element method. An initial mesh sensitivity analysis showed that good refinement is essential for obtaining more accurate results. The parametric analysis results reinforce the importance of careful calibration of the parameters of the constitutive model, since small changes can significantly impact the initiation and propagation of fractures in the damage zones. The results obtained in this study make it possible to evaluate the generation of fracture networks in the vicinity of the fault, demonstrating the relevance of the methodology adopted.

Keywords: Numerical modeling, Geological faults, Fracturing, Finite elements.

1 Introduction

Geological faults are complex structures formed by different deformation mechanisms in rocks. These structures are made up of a core and an adjacent damage zone. The core, filled with degraded rock, typically represents a barrier to fluid flow[1]. On the other hand, damage zones have different structures depending on the type of rock. Very porous rocks such as sandstones can undergo grain breakage and reorganization as well as pore collapse, resulting in different kinds of deformation bands that reduce permeability in the damage zones. On the other hand, rigid, low-porosity rocks such as carbonates can generate isolated fractures or networks of fractures that considerably increase the rock's permeability [2], [3], [4], [5].

Recent studies have presented different techniques for modeling fractured regions in geological media, showing significant advances in understanding these phenomena[6]. However, a good representation of fractures in continuous media has substantial limitations, since these discontinuities cannot be directly incorporated into the

traditional formulation of the continuum. To overcome this restriction and improve the analysis of the fracture formation and development process, this study proposes a methodology for numerical modeling of geological faults that combines continuous finite elements with cohesive interface elements throughout the finite element mesh to represent possible fractures explicitly.

To assess the influence of this approach, a mesh sensitivity analysis is initially carried out to evaluate the response of the interface elements to different discretizations and compared with a continuous damage zone methodology using equivalent plastic deformations. A parametric study is conducted to evaluate different simulation scenarios. Three main steps will be considered: initially, the effect of normal and tangential stiffness will be analyzed, followed by the variation of maximum stress values associated with the onset of damage, and finally, different levels of fracture energy will be tested. Finally, the results will be compared to analyze each parameter's effect on the fractured region's mechanical behavior.

2 Methodology

In this study, the vertical section of a reservoir containing a normal fault is modeled under plane strain conditions. The fault is represented by a discontinuity composed of two phases under which opposite displacements are imposed, as shown in Figure 1. These displacements are imposed incrementally according to a parabolic distribution with zero displacements at the ends and maximum displacement (dmax) at the center of the fault. The value of $dmax$ is defined as 10% of the total fault length (L), see values observed in the literature[7]. The displacements at the model's edges are restricted in horizontal and vertical directions, and the edges are sufficiently far from the discontinuity to avoid edge effects in the results. The finite element mesh consists of triangular elements (CPE3) and interface elements (COH2D4) inserted on each edge of the triangular elements. All elements are linear, and the full integration is considered (one and two integration points for triangles and interface elements, respectively).

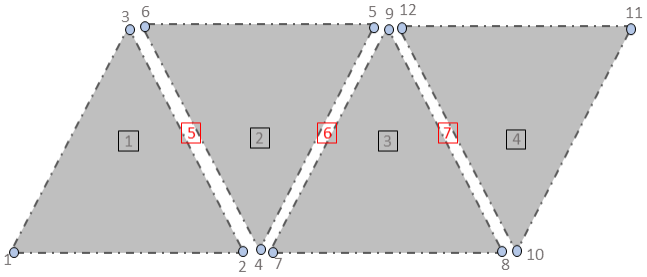


Figure 1 - Mesh with continuous and discrete elements

The linear elastic constitutive model is chosen to analyze the rock's geomechanical behavior as expressed by Hooke's law ($\boldsymbol{\sigma} = \boldsymbol{D} \cdot \varepsilon$) where σ is the stress tensor, ε is the deformation vector, and $\boldsymbol{D}$ is the elastic constitutive tensor defined from Young's modulus (E) and Poisson's ratio (ν).

The constitutive model used to analyze the discontinuities in the interface elements is the Cohesive Zone Model (CZM). The CZM is used to simulate the initiation and propagation of fractures through a traction-separation constitutive relationship (Figure 2) that describes the relative displacement and traction in the element through a characteristic curve [8].

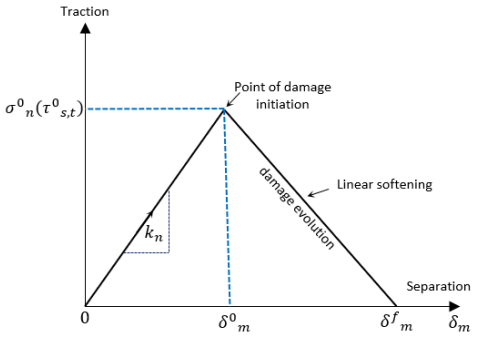


Figure 2 – Cohesive Zone Model (CZM). $\sigma^0{}_n(\tau^0{}_{s,t})$ is the maximum normal and shear stress before damage, $\delta^0{}_m$ is the relative displacement at which damage begins, $\delta^f{}_m$ refers to the deformation where the damage is complete and k_n is the normal stiffness, represented by the initial slope of the traction-separation curve.

Damage initiation refers to the beginning of the degradation of the response at a material point. The degradation process begins when the stresses and strains meet specific criteria. Here, the initiation of the damage process is predicted using the maximum stress criterion, see Eq. 1, i.e. damage begins when the maximum value of the ratio between the stress t and the nominal stress (t_n, t_s, t_t) (resistance) at a point reaches a value of 1.

$$máx.\left\{\frac{\langle t_n \rangle}{t^0{}_n}, \frac{t_s}{t^0{}_s}, \frac{t_t}{t^0{}_t}\right\} = 1 \tag{1}$$

The material's stiffness is then progressively degraded using a damage variable D, whose evolution is determined by a softening law (Eq.2) based on the effective displacements.

$$D = \frac{\delta^f{}_m(\delta^{max}{}_m - \delta^0{}_m)}{\delta^{max}{}_m(\delta^f{}_m - \delta^0{}_m)} \tag{2}$$

Different mechanisms, such as displacement and energy, can represent the evolution of damage. This study used an evolution law based on fracture energy, corresponding to the area under the stress-separation curve. The Benzeggagh-Kenane model [9] is used to simulate the evolution of damage during the fracture propagation process. This criterion is applicable when the critical fracture energies of the rock material along the first and second shear directions are similar, i.e., $G_s{}^c = G_t{}^c$. The critical energy considers the mixed damage mechanism, i.e., combined in multiple directions, as shown below (Eq. 3):

$$G^c = G^c{}_n + (G^c{}_s - G^c{}_n)\left\{\frac{G_S}{G_T}\right\}^\eta \tag{3}$$

where $G^c{}_n$ e $G^c{}_s$ are the mode I and mode II critical fracture energies, respectively; $G_S = G_s + G_t$, $G_T = G_n + G_S$. G_n, G_s and G_t are the work done by the tractions and their conjugate relative displacements in the normal, first and second shear directions, respectively, and η is a material parameter. This paper adopts η = 2,284 [10].

The workflow developed follows a conventional procedure: definition of the geometry, boundary conditions, and properties, generation of the continuous mesh, fragmentation of the mesh using MeshFrag[10], simulation, and, finally, analysis and interpretation of the results using Abaqus software.

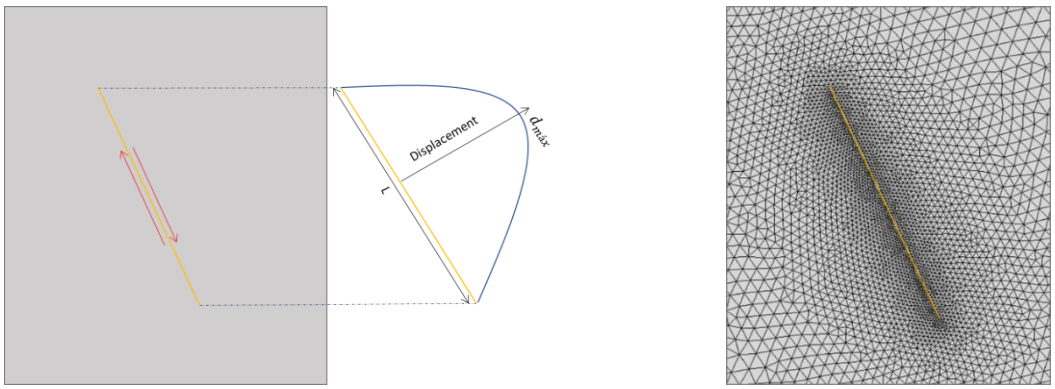
3 Numerical Tests

In the numerical simulations presented here, a normal fault with a length of 1000 meters and an inclination angle of 65° is modeled at the center of the domain. Table 1 lists the geomechanical parameters used for the proposed analyses and Figure 3 (a, b) shows the model geometry, imposed displacements, and mesh, respectively.

The vertical stress gradient is 0.010MPa/m for the continuous elements. The horizontal stresses are obtained from the vertical ones, considering a stress ratio 0.9.

Table 1. Rock parameters

Parameters	Nomenclature	Value
Young's modulus	E	$1.7 \cdot 10^{10} Pa$
Poisson's ratio	ν	0.20
Normal stiffness of the fracture	k_n	$1.7 \cdot 10^{11} Pa/m$
Shear stiffness in two directions of the fracture	k_s, k_t	$7.08 \cdot 10^{10} Pa/m$
Effective tensile strength	${\sigma^0}_n$	$1.250 \cdot 10^6 Pa$
Shear strengths	${\tau^0}_{s,t}$	$5.0 \cdot 10^6 Pa$
Fracture energy	G^c	$120\ N/m$

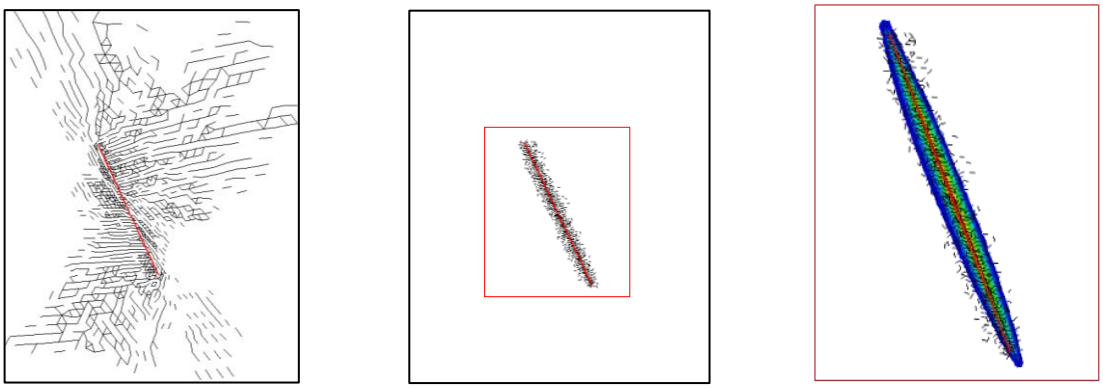


(a) (b)

Figure 3 - Model geometry and displacements imposed over the two faces of the fault (a) and the finite element mesh (b).

3.1 Mesh sensitivity study

Different discretizations were used to study the impact of the mesh on the results. Initially, the model was built with 50 and 100 elements along the fault discontinuity. In addition, a mesh generation with a refinement gradient was adopted, in which the discretization becomes progressively coarser as it moves away from the fault region, capturing stress concentrations while optimizing computational cost. Figure 4 illustrates the damage results for the two discretization orders. It can be observed that, in the 50-element mesh, the fractures along the fault exhibit an irregular pattern and extend to the upper boundary of the model, causing instability (hyperstaticity) in the analysis. In contrast, the results obtained for the 100-element model are more consistent, indicating that the displacement applied along the fault influences the formation of the fractured zone. A higher concentration of fractures near the discontinuity indicates behavior compatible with the expected mechanisms. Furthermore, when comparing this configuration with a continuous approach, it can be seen that the boundaries of the fractured zone are similar to those observed in damage zones generated by continuous models based on equivalent deformations.



(a) (b) (c)

Figure 4 – Fractured region results for different mesh discretizations: (a) model with 50 elements, (b) model with 100 elements, and (c) overlap of solutions obtained with the refined mesh (100 elements), comparing the cohesive and continuous (elastoplastic) modeling approaches.

3.2 Parametric analysis

In order to understand the sensitivity of the model to the parameters adopted in the behavior of the cohesive elements, several numerical analyses were carried out. Initially, the influence of the normal and tangential stiffness moduli in the cohesive model on the overall behavior of the structure was evaluated. Next, the effects of varying the maximum stress values associated with the onset of damage were analyzed, observing their influence on fracture nucleation. Finally, simulations were carried out varying the values of fracture energy to understand its contribution to the propagation of discontinuities. The elastic parameters of the continuous elements were the same as those described in Table 1. The values used in the parametric study are detailed in Table 2.

Table 2. Analyzed parameters in the cohesive model

Parameters	Nomenclature	Value 1	Value 2
Normal stiffness	k_n	$1.7 \cdot 10^{11} Pa/m$	$1.7 \cdot 10^{12} Pa/m$
Shear stiffness	k_s, k_t	$7.08 \cdot 10^{10} Pa/m$	$7.08 \cdot 10^{11} Pa/m$
Effective tensile strength	${\sigma^0}_n$	$1.250 \cdot 10^6 Pa$	$1.250 \cdot 10^9 Pa$
Shear strength	${\tau^0}_{s,t}$	$5.0 \cdot 10^6 Pa$	$5.0 \cdot 10^9 Pa$
Fracture energy	G^c	$1.2 \cdot 10^2\ N/m$	$1.2 \cdot 10^3\ N/m$

The first set of analyses corresponds to the variation in the normal and tangential stiffness of the cohesive model. The results shown in Figure 5 indicate that increasing the normal stiffness modulus resulted in higher fracture concentrations in the region adjacent to the fault, contributing to the increased fracture density observed. This behavior occurs because higher stiffness moduli result in higher stresses, causing longer elements to reach the rupture criterion. Consequently, more fractures can be observed, even in regions further away from the fault.



(a) (b)

Figure 5 - Results for different values of normal and shear stiffness (a) value 1 ($k_n = 1.7 \cdot 10^{11} Pa/m, k_s, k_t = 7.08 \cdot 10^{10} Pa/m$) and (b) value 2 ($k_n = 1.7 \cdot 10^{12} Pa/m, k_s, k_t = 7.08 \cdot 10^{11} Pa/m$) of the table 2.

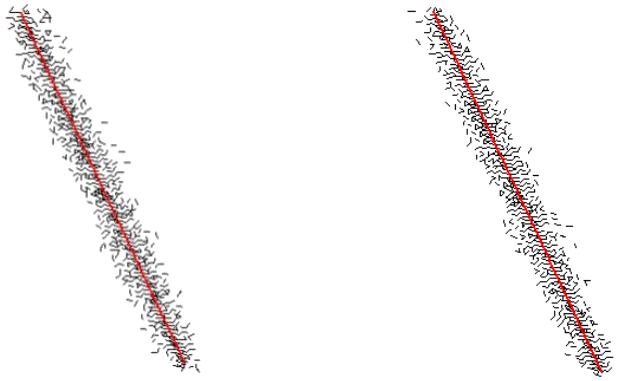
The results shown in Figure 6 refer to the analysis of the variation in the maximum normal and shear stress values associated with the onset of damage in the cohesive elements. It can be seen that for higher limit stress values, the number of fractured interface elements is significantly lower. This behavior can be explained by the higher the nominal stress value for damage initiation, the greater the stress path required for the material degradation process to begin. As a result, when damage starts to occur, the model is already subjected to higher stress levels, slowing down the propagation of fractures and reducing the extent of the damaged regions.



(a) (b)

Figure 6 - Results for different values of adequate tensile and shear strength (a) value 1 $({\sigma^0}_n = 1.250 \cdot 10^6 Pa, {\tau^0}_{s,t} = 5.0 \cdot 10^6 Pa)$ and (b) value 2 $({\sigma^0}_n = 1.250 \cdot 10^9 Pa, {\tau^0}_{s,t} = 5.0 \cdot 10^9 Pa)$ of the table 2.

The results illustrated in Figure 7 correspond to the analysis of the variation of the different fracture energy values adopted in the model. In general, the differences between the scenarios were not significant at the final stage of the simulation. However, when analyzing the process's evolution over the simulation, there is a distinct behavior between the cases. For lower fracture energy values, damage growth is more contained, with the fracture generation rate stabilizing after approximately 60% of the total applied load. On the other hand, for higher fracture energy values, the appearance of fractures occurs more gradually and continuously throughout the simulation, indicating a more progressive and distributed damage process.



(a) (b)

Figure 7 – Fracture energy results for different values of normal and shear stiffness (a) value 1 $(G^c = 1.2 \cdot 10^2\ N/m)$ and (b) value 2$(G^c = 1.2 \cdot 10^3\ N/m)$ of the table 2.

4 Conclusions

This study uses cohesive elements and discrete fracture representation to evaluate the influence of mesh discretization and cohesive zone model parameters on the initiation and propagation of fractures around a geological fault. It was found that using a more refined mesh along the fault contributes to the stabilization of the interface elements, providing a more accurate response when compared to the results of damage zones in continuous models. The parametric analysis observed that higher values of normal and tangential stiffness favor

the concentration of stress and the formation of more intense fractured zones. As for the nominal stress values for damage initiation, high values delay damage activation due to the rock's greater resistance, reducing the fractured region's extent. Finally, the fracture energy analysis revealed that higher values lead to a more controlled damage evolution, with stabilization in fracture formation, characterizing a more ductile material response. On the other hand, for lower levels of fracture energy, the behavior observed is more fragile, with fractures developing more abruptly and less distributed throughout the analysis. These results reinforce the importance of properly calibrating the parameters and the mesh when modeling fracturing processes in continuous media.

Acknowledgements. This research was carried out in association with the ongoing R&D project registered as ANP nº 21475-9, "GeoBanD 2 – Geomodelagem de zona de dano em falhas geológicas" (PUC-Rio/CENPES/ANP), sponsored by Petrobras. The authors also gratefully acknowledge the support from Carlos Chagas Filho Foundation for Supporting Research in the State of Rio de Janeiro (FAPERJ) Grant E-26/211.766/2021-0, Brazilian National Council for Scientific and Technological Development (CNPq) Grants 141617/2020-9, 420074/2021, and 407388/2022-2, Department of Civil Engineering and Environment, and Tecgraf Institute from PUC-Rio.

Authorship statement. The authors hereby confirm that they are the sole liable persons responsible for the authorship of this work, and that all material that has been herein included as part of the present paper is either the property (and authorship) of the authors, or has the permission of the owners to be included here.

References

[1] H. Fossen, *Structural geology*, vol. 1, no. 1. Cambridge university press, 2016.

[2] P. A. Cowie and C. H. Scholz, "Physical explanation for the displacement-length relationship of faults using a post-yield fracture mechanics model," *J. Struct. Geol.*, vol. 14, no. 10, pp. 1133–1148, 1992, doi: 10.1016/0191-8141(92)90065-5.

[3] Y. S. Kim, D. C. P. Peacock, and D. J. Sanderson, "Fault damage zones," *J. Struct. Geol.*, vol. 26, no. 3, pp. 503–517, 2004, doi: 10.1016/j.jsg.2003.08.002.

[4] A. G. McGrath and I. Davison, "Damage zone geometry around fault tips," *J. Struct. Geol.*, vol. 17, no. 7, pp. 1011–1024, 1995, doi: 10.1016/0191-8141(94)00116-H.

[5] H. Fossen, *Structural Geology*. Cambridge University Press, 2010. doi: 10.1017/CBO9780511777806.

[6] M. Johri, E. M. Dunham, M. D. Zoback, and Z. Fang, "Predicting fault damage zones by modeling dynamic rupture propagation and comparison with field observations," *J. Geophys. Res. Solid Earth*, vol. 119, no. 2, pp. 1251–1272, Feb. 2014, doi: 10.1002/2013JB010335.

[7] R. Quevedo, T. J. de Andrade, L. Santos, B. R. B. M. Carvalho, and D. Roehl, "Assessment of fault damage zones in carbonate rocks based on numerical and sensitivity analyses," *Tectonophysics*, vol. 864, no. March, p. 230023, 2023, doi: 10.1016/j.tecto.2023.230023.

[8] P. P. Camanho and C. G. Davila, "Mixed-Mode Decohesion Finite Elements for the Simulation of Delamination in Composite Materials," *NASA Tech. Pap.*, vol. 211737, no. June, p. 42, 2002, [Online]. Available: http://citeseerx.ist.psu.edu/viewdoc/download?doi=10.1.1.8.267&rep=rep1&type=pdf

[9] M. L. Benzeggagh and M. Kenane, "Measurement of mixed-mode delamination fracture toughness of unidirectional glass/epoxy composites with mixed-mode bending apparatus," *Compos. Sci. Technol.*, vol. 56, no. 4, pp. 439–449, 1996, doi: 10.1016/0266-3538(96)00005-X.

[10] J. A. R. Cordero, "Failure phenomena and fluid migration in naturally fractured rock formations," 2021.